

Electronic Supplementary Information

Solar Fuels Photoanodes Prepared by Inkjet Printing of Copper Vanadates

P. F. Newhouse,^a D. A. Boyd,^{ab} A. Shinde,^a D. Guevarra,^a L. Zhou,^a E. Soedarmadji,^a G. Li,^c J. B. Neaton,^{cd} J. M. Gregoire^{*a}

Images of inkjet-printed samples

Figure 3 contains an image of a 2×59.2 mm region of a library plate that contains the 26-sample library covering the full composition range of $\text{Cu}_{1-x}\text{V}_x\text{O}_z$ with 0.04 intervals in x . The systematic arrangement of the samples was used for intuitive visualization of the Raman imaging results. For UV-vis and photoelectrochemistry characterization, the composition samples were randomized within each 26-sample set. Figure S1 shows 10 copies of the 26-sample composition library where an image of each sample was extracted from the library plate image. The 260 sample images are ordered with respect to composition, demonstrating the excellent reproducibility in the optical properties of each composition in duplicate libraries. An occasional defective sample is observed, which may be due to poor adhesion of the calcined material due to surface contamination; the possibility of a false negative result from such defective samples motivated the 3-fold duplicate measurements and data averaging scheme for photoelectrochemical characterization.

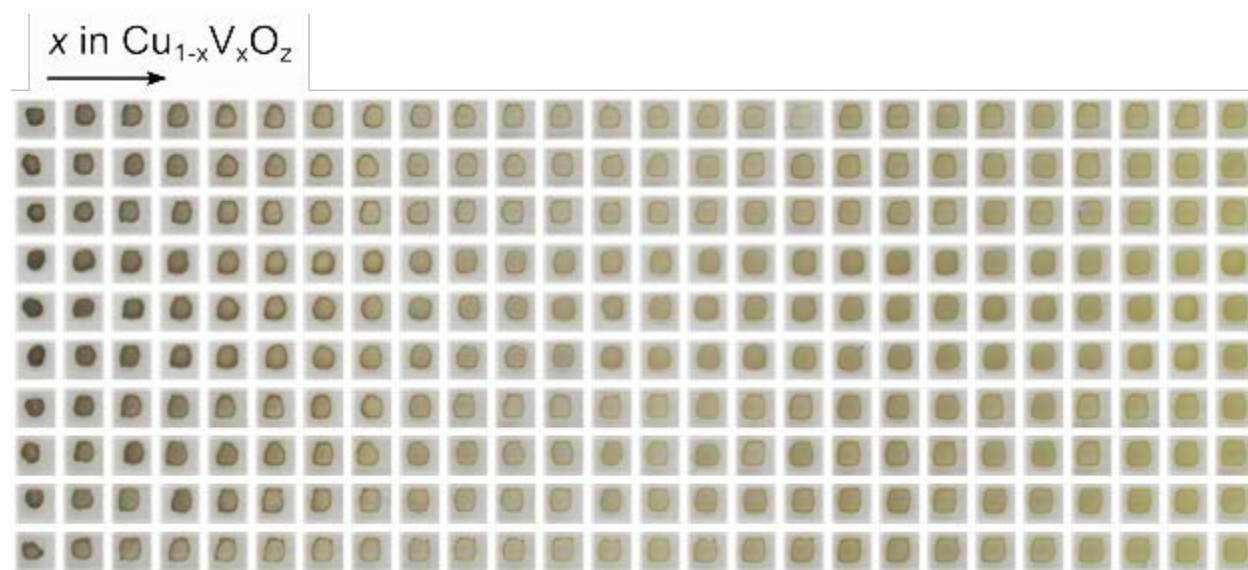


Figure S1: 260 sample images of inkjet-printed samples, horizontally arranged in order of increasing V concentration. The 10 image vertical stack at each composition are duplicate composition samples from a single library plate, which were used for making duplicate measurements and photoelectrochemical measurements in different electrolytes.

Raman calculations and phase identification

Figure S2 shows Raman patterns for the following 4 phases, where the citations indicate the source of the reference patterns: $\beta\text{-Cu}_3\text{V}_2\text{O}_8$ (no reference pattern available), $\gamma\text{-Cu}_3\text{V}_2\text{O}_8$,¹ $\beta\text{-Cu}_2\text{V}_2\text{O}_7$ ² (RRUFF ID:

R070482), α -Cu₂V₂O₇.¹ For the latter 2 phases, the representative spectrum from the post-RTP library is shown, which are also shown in Figure 2. Given the excellent match between our experimental spectra in the $x = 0.36$ composition region and the β -Cu₂V₂O₇ reference pattern, and the dissimilarity between these experimental spectra and the γ -Cu₃V₂O₈ reference pattern (the photoelectrocatalyst phase we obtained using PVD synthesis at this composition), the only conclusion from the available experimental data is that our material indeed has the β -Cu₂V₂O₇ structure.

To support this hypothesis, we calculated the Raman patterns of the 4 phases in Figure S2. All the density functional theory (DFT) calculations are performed with VASP,¹⁻⁴ using the Perdew-Burke-Ernzerhof (PBE) exchange-correlation functional.³ These calculations used a plane-wave basis and projector augmented-wave (PAW) potentials,^{4,5} requiring a plane-wave cutoff of 520 eV. The calculations were spin polarized, and a Hubbard-type U term⁶ was used to address the on-site Coulomb interactions in the d states. The U values for Cu and V were 6.52 eV and 3.10 eV, respectively. In the calculations of the bulk structures of γ -Cu₃V₂O₈ (mp-504747), β -Cu₃V₂O₈ (mp-600273), α -Cu₂V₂O₇ (mp-505508), and β -Cu₂V₂O₇ (mp-559660), the k -meshes were 6×6×5, 5×4×5, 4×4×2, and 5×5×3, respectively. The bulk structures were fully relaxed until the forces on each atom are less than 0.001 eV/Å. The calculated lattice constants of the four phases are $a=5.21$ Å, $b=5.46$ Å, $c=6.62$ Å, $\alpha=110.65^\circ$, $\beta=88.32^\circ$, $\gamma=111.65^\circ$; $a=6.31$ Å, $b=8.08$ Å, $c=6.52$ Å, $\alpha=\gamma=90^\circ$, $\beta=110.84^\circ$; $a=b=5.47$ Å, $c=10.85$ Å, $\alpha=\beta=100.20^\circ$, and $\gamma=107.35^\circ$; $a=b=5.65$ Å, $c=10.25$ Å, $\alpha=\beta=103.73^\circ$, and $\gamma=92.08^\circ$, respectively. Using these optimized structures, we calculated the Raman spectra using the script `vasp_raman.py`.⁷

The Raman-active modes are plotted in Figure S2 with a square-root intensity scale to promote visualization of the weaker Raman modes. For the 3 phases with available reference patterns (γ -Cu₃V₂O₈, β -Cu₂V₂O₇, α -Cu₂V₂O₇), the calculated patterns are systematically shifted to lower wavenumber compared to the experimental patterns, which is typical for calculated Raman spectra, and otherwise match very well with the experimental patterns. Of particular interest is the calculated pattern for the β -Cu₃V₂O₈ phase since the stoichiometry of this phase is similar to that of our $x = 0.36$ region of interest. This phase was recently reported as an OER photoelectrocatalyst,⁸ and there is no available reference pattern. The calculated pattern shows that the Raman signal from this phase is markedly different from that of β -Cu₂V₂O₇, and it is thus implausible that we have a majority of this phase at the $x = 0.36$ composition region. For the β -Cu₂V₂O₇ phase, the cluster of peaks in the 750-950 cm⁻¹ range appear to have different relative intensities in our experimental pattern, the mineral reference pattern, and the calculated Raman pattern. Given that both β -Cu₃V₂O₈ and γ -Cu₃V₂O₈ exhibit peaks in this range, it is possible that small amounts of these phases are mixed with the β -Cu₂V₂O₇ structure in the inkjet-printed libraries. One important indication that the β -Cu₂V₂O₇ phase is indeed the primary phase arises from inspection of the Raman signals at wavenumbers above the strongest peak in each phase. The calculated patterns reveal that only β -Cu₂V₂O₇ exhibits a Raman-active mode with appreciable intensity in this wavenumber range, which is circled in Figure S2 and clearly observed in our experimental data.

While Figures 2 and S2 contain representative spectra from both the as-calcined and post-RTP Raman imaging datasets, only the post-RTP phase distribution is shown in Figure 3. Figure S3 shows as-calcined sample images and false-colour map of phase distribution for the 6 reference patterns and the FTO/glass substrate. This is analogous to Figure 4 and no substantial difference between the phase-distributions were observed.

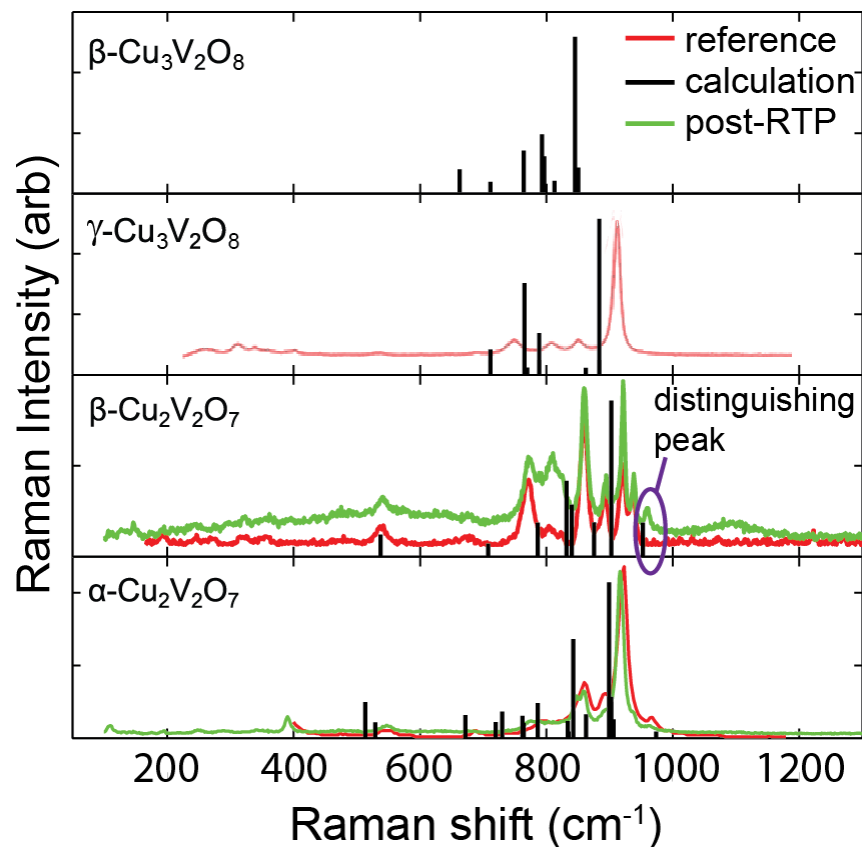


Figure S2: The results of the Raman pattern calculations for 4 copper vanadate phases is shown (black lines) with the height of each line corresponding to the square-root of the relative intensity of the Raman mode. The available reference patterns are shown as well as the representative post-RTP spectra from Figure 2.

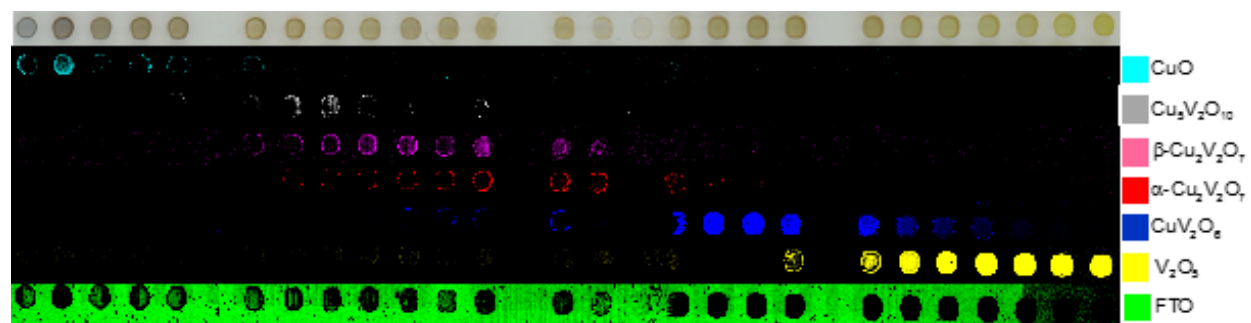


Figure S3: Analogous data to that of Figure 4 (post-RTP library) for an as-calcined library. The data quality from this Raman imaging dataset is of lower quality than the post-RTP library, but by applying the same data analysis and phase distribution visualization the same phase behaviour is observed in both libraries.

UV-vis data for representative composition samples

Figure 5 shows the spectral absorption coefficient ($\alpha \times t$) for several compositions in the as-calcined library and additionally shows the direct-allowed (DA) Tauc plot for the 3 representative copper vanadate samples from the as-calcined and post-RTP library. To provide additional visualization of the

differences in optical properties between the as-calcined and post-RTP samples, absorption coefficient (Figure S4) and indirect-allowed Tauc spectrum (Figure S5) are shown for the 3 representative copper vanadate samples.

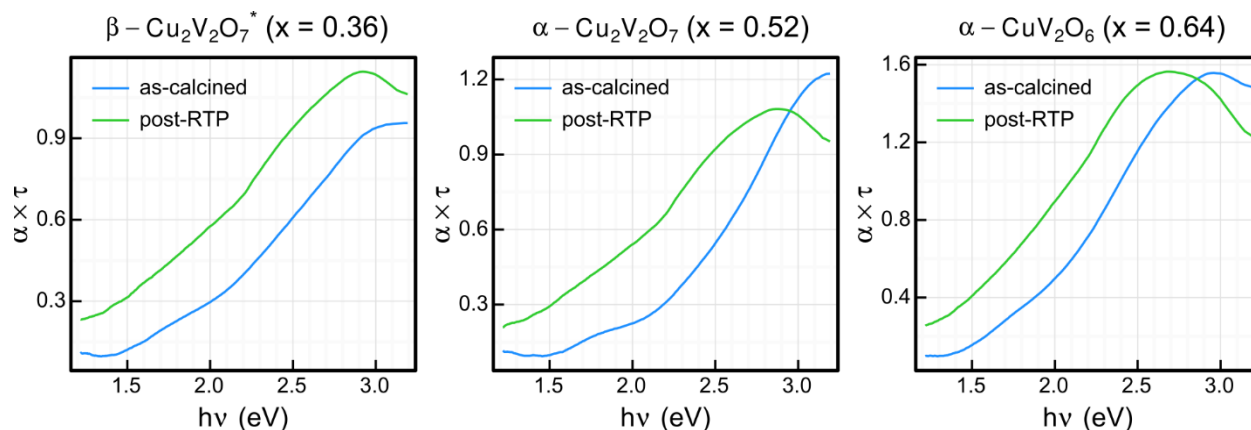


Figure S4: The spectral absorption coefficient from UV-vis measurements for the 3 representative copper vanadate composition samples from both as-calcined and post-RTP libraries.

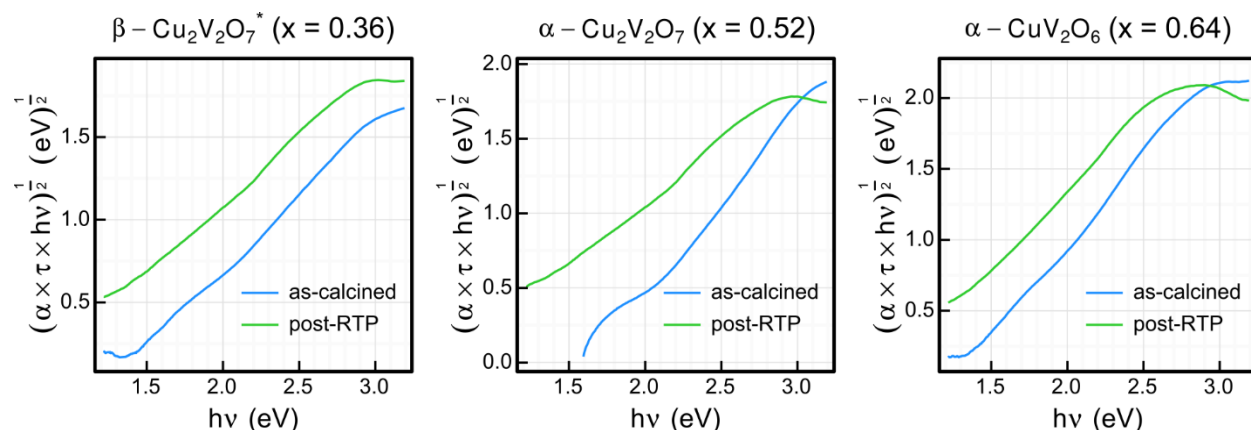


Figure S5: The indirect-allowed Tauc spectra from UV-vis measurements for the 3 representative copper vanadate composition samples from both as-calcined and post-RTP libraries.

1. T. Kawada, S. Hinokuma and M. Machida, *Catal. Today*, 2015, **242**, 268-273.
2. L. B, D. R. T, Y. H and S. N, in *Highlights in Mineralogical Crystallography*, eds. T. Armbruster and R. M. Danisi, W. De Gruyter, Berlin, Germany, 2015, pp. 1-30.
3. J. P. Perdew, K. Burke and M. Ernzerhof, *Phys. Rev. Lett.*, 1996, **77**, 3865-3868.
4. G. Kresse and D. Joubert, *Phys. Rev. B*, 1999, **59**, 1758.
5. P. E. Blochl, *Phys. Rev. B*, 1994, **50**, 17953-17979.
6. S. L. Dudarev, G. A. Botton, S. Y. Savrasov, C. J. Humphreys and A. P. Sutton, *Phys. Rev. B*, 1998, **57**, 1505.
7. A. Fonari and S. Stauffer, in *vasp_raman.py*, <https://github.com/raman-sc/VASP/>, 2013.
8. J. A. Seabold and N. R. Neale, *Chem Mater*, 2015, DOI: 10.1021/cm504327f, 150112115329007.